Mineralogical Magazine, December 2012, Vol. 76(7), pp. 2837–2860

Crystal structure and formula revision of deliensite, $Fe[(UO_2)_2(SO_4)_2(OH)_2](H_2O)_7$

J. Plášil[1,*], J. Hauser[2], V. Petříček[1], N. Meisser[3], S. J. Mills[4], R. Škoda[5], K. Fejfarová[1], J. Čejka[6], J. Sejkora[6], J. Hloušek[7], J.-M. Johannet[8], V. Machovič[9,10] and L. Lapčák[9]

[1] Institute of Physics ASCR, v.v.i., Na Slovance 2, CZ-18221 Prague 8, Czech Republic
[2] Department of Chemistry and Biochemistry, University of Bern, Freiestrasse 3, CH-3012 Bern, Switzerland
[3] Musée de Géologie and Laboratoire des Rayons-X, Institut de Minéralogie et de Géochimie, UNIL, Anthropole, CH-1015 Lausanne-Dorigny, Switzerland
[4] Geosciences, Museum Victoria, GPO Box 666, Melbourne, Victoria 3001, Australia
[5] Department of Geological Sciences, Faculty of Science, Masaryk University, Kotlářská 2, CZ-611 37, Brno, Czech Republic
[6] Department of Mineralogy and Petrology, National Museum, Cirkusová 1740, 193 00 Prague 9 - Horní Počernice, Czech Republic
[7] U Roháčových kasáren 24, CZ-100 00, Praha 10, Czech Republic
[8] Richemont, F-79250 Nueil-les-Aubiers, France
[9] Institute of Chemical Technology, Prague, Technická 5, CZ-16628, Prague 6, Czech Republic
[10] Institute of Rock Structures and Mechanics ASCR, v.v.i., V Holešovičkách 41, CZ-18209, Prague 8, Czech Republic

[*Received 15 July 2012; Accepted 1 November 2012; Associate Editor: Giancarlo Della Ventura*]

ABSTRACT

The crystal structure of deliensite, $Fe[(UO_2)_2(SO_4)_2(OH)_2](H_2O)_7$, was solved by direct methods and refined to $R_1 = 6.24\%$ for 5211 unique observed reflections [$I_{obs} > 3\sigma(I)$], on a crystal that was found to consist of rotational and inversion (merohedral) twins, from Jeroným mine, Abertamy in the Czech Republic. The presence of four twin domains was taken into account in the refinement. The structure is orthorhombic, space group *Pnn*2, with unit-cell parameters a = 15.8514(9), b = 16.2478(7), c = 6.8943(3) Å, V = 1775.6(1) Å^3 and Z = 4. The crystal structure of deliensite contains uranyl-sulfate sheets with a phosphuranylite topology, consisting of dimers of edge-sharing uranyl pentagonal bipyramids linked by corner-sharing with sulfate tetrahedra. The sheets lie in the (100) plane and are decorated by $[Fe^{2+}O(H_2O)_5]$ octahedra; two weakly bonded H_2O molecules are present in the interlayer. The $[Fe^{2+}O(H_2O)_5]$ octahedron is linked directly to the sheet via the uranyl oxygen atom. Adjacent sheets are linked by hydrogen bonds only. The sheet topology and geometrical isomerism is discussed and a comparison of the composition obtained from electron-probe microanalysis, powder-diffraction data, Raman and infrared spectra of deliensite samples from Mas d'Alary, Lodève, France; L'Ecarpière mine, Gétigné, France; and several localities at Jáchymov, Western Bohemia, Czech Republic is made.

Keywords: uranyl sulfate, crystal structure, phosphuranylite topology, Raman spectroscopy, infrared spectroscopy.

Introduction

Uranyl sulfate minerals are commonly formed as alteration products of primary U^{4+}-bearing phases (Finch and Murakami, 1999) if a suitable source of SO_4^{2-} anions is available (e.g. by the

* E-mail: plasil@fzu.cz
DOI: 10.1180/minmag.2012.076.7.14

oxidation of pyrite, marcasite or other simple sulfides). They commonly occur at abandoned and active uranium mines, where they may precipitate in areas affected by acid mine drainage (AMD) or other acidic groundwater; in mine dumps; and in the supergene oxidation zones of uranium-rich deposits (e.g. Ondruš *et al*., 1997; Meisser *et al*., 2002; Brugger *et al*., 2003; Mills *et al*., 2008*a*,*b*; Plášil *et al*., 2008, 2011*a*,*b*; Birch *et al*., 2011). Detailed studies of uranyl sulfates are of importance as they are possible alteration phases in future repositories for radioactive waste (e.g. Jensen *et al*., 2002; Deditius *et al*., 2008; Oelkers and Montel, 2008). A detailed knowledge of the crystal chemistry of uranyl minerals is necessary in evaluating their potential to immobilize, temporarily store and release uranium and other environmentally harmful elements. This information is also needed for thermodynamic modelling and mineral stability calculations (e.g. Chen *et al*., 1999; Schindler and Hawthorne, 2008). Relatively few uranyl sulfate mineral structures have been solved. Those that have include johannite (Mereiter, 1982), the mixed sulfate-carbonate mineral schröckingerite (Mereiter, 1986), uranopilite (Burns, 2001), marécottite (Brugger *et al*., 2003), sejkoraite-(Y) (Plášil *et al*., 2011*a*), zippeite (Plášil *et al*., 2011*b*), adolfpateraite (Plášil *et al*., 2012*a*), pseudojohannite (Plášil *et al*., 2012*b*), magnesiozippeite (Plášil *et al.*, 2012*c*) and natrozippeite (authors' unpublished data).

Deliensite was described as a new mineral with an ideal formula $Fe(UO_2)_2(SO_4)_2(OH)_2(H_2O)_3$ from the Mas d'Alary uranium deposit, Lodève, France (Vochten *et al*., 1997). The composition of the structural unit, $[(UO_2)_2(SO_4)_2(OH)_2]^{2-}$, reported by Vochten *et al*. (1997), is identical to that of johannite, $Cu[(UO_2)_2(SO_4)_2(OH)_2](H_2O)_8$, although the original description did not include a structure determination, due to the small size of the crystals from the type locality.

In the current paper we present the first report of the crystal structure of deliensite from single-crystal X-ray diffraction data and discuss the composition and structure of the mineral from several worldwide localities.

Specimens

Deliensite crystals from three different localities were used in the single-crystal X-ray diffraction experiments. The crystal for which the crystal structure was solved was found at the Jeroným mine, Abertamy deposit, Jáchymov ore district, Western Bohemia, Czech Republic. The specimen ($8 \times 4 \times 2$ cm) contains a rich uraninite vein with granular pyrite or marcasite, both of which are strongly altered. Rich crystalline aggregates of deliensite occur with rozenite, melanterite and jarosite on the surface of the specimen and in fractures (Fig. 1). These aggregates consist of intergrown prismatic deliensite crystals elongated

FIG. 1. Elongated prismatic deliensite with jarosite (yellowish) melanterite (colourless with a glassy lustre) on strongly altered uraninite from Jeroným mine, Abertamy deposit, Jáchymov ore district, Western Bohemia, Czech Republic. Field of view 2.5 mm (photo by P. Škácha).

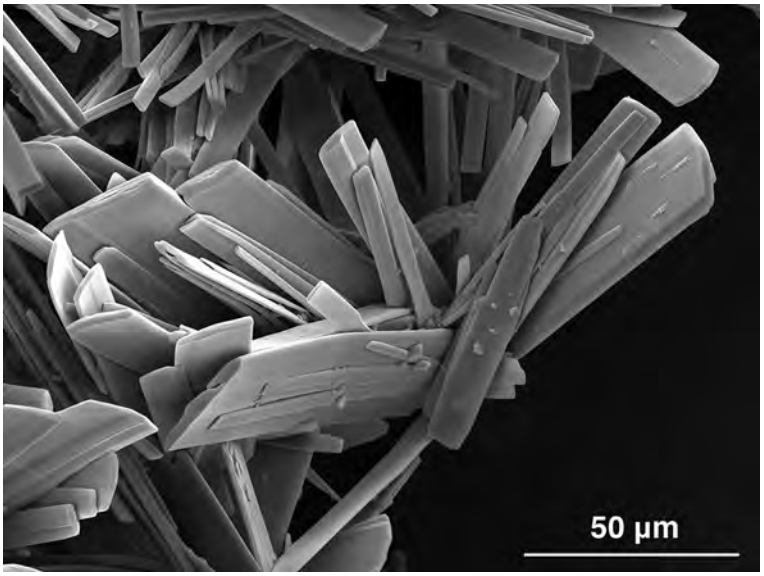

FIG. 2. Aggregate of prismatic [001] deliensite crystals from Jeroným mine, Abertamy deposit, Jáchymov ore district, Western Bohemia, Czech Republic (sample MGL 92633).

on [001] or thin tabular crystals on {100} and show the forms (100), (120), (010), (001) and (011) (Fig. 2). The cleavage on {100} is perfect (Fig. 3).

A specimen from the type locality for deliensite, the Mas d'Alary uranium deposit, Lodève, France (Vochten *et al*., 1997; Caubel, 1998), which was originally in the collection of Michel Deliens, was studied by single-crystal X-ray diffraction and wavelength-dispersive spectrometry (WDS). This specimen ($0.5 \times 1 \times 1$ cm) is a fragment of pyrite with disseminated uraninite, coated in small orthorhombic deliensite crystals.

Several samples of deliensite from the Jáchymov area were studied, including rich specimens from the dumps of Schweitzer mine (labelled S) and Geister mine (labelled G). Specimen S ($4 \times 3 \times 2$ cm) consists of massive altered dark red-brown to blackish uraninite coated in supergene deliensite and uranopilite crystals (Fig. 4). Specimen G consists of disseminated uraninite in a highly altered gangue penetrated by small cracks filled with gypsum; on this specimen deliensite occurs with johannite and zippeite (Fig. 5).

Deliensite from a relatively recent find at the L'Ecarpière mine, Gétigné, Loire Atlantique, France was studied by powder X-ray diffraction and energy-dispersive spectrometry (EDS). The mine, which is near the hamlet of Gétigné, was the most productive uranium mine (producing 4109 tonnes of uranium metal; Chapot *et al.*, 1996) in the COGEMA (now AREVA) Vendée district. It was worked opencast and underground between 1956 and 1990. The main uranium ore was uraninite (pitchblende), accompanied by fluorite, pyrite and marcasite. Acid mine drainage

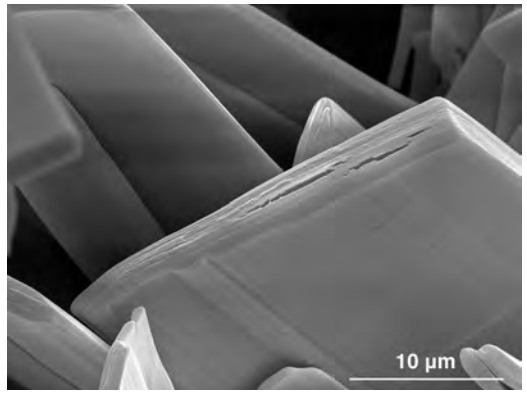

FIG. 3. Perfect {100} cleavage of deliensite from Jeroným mine, Abertamy deposit, Jáchymov ore district, Western Bohemia, Czech Republic (sample MGL 92633).

FIG. 4. Long prismatic crystals of deliensite on altered uraninite from Schweizer mine, Jáchymov ore district, Western Bohemia, Czech Republic. Field of view 3 mm (photo by P. Škácha).

caused by pyrite decomposition has led to the formation of abundant *in situ* uranopilite. The studied specimen was collected from the main stockpile and consists of massive highly altered uraninite with gypsum and other secondary minerals including deliensite and natrozippeite, which were identified by powder XRD and EDS. Deliensite occurs as brown to orange-brown crystalline aggregates covering an ~2 × 1 cm area of the specimen (Fig. 6). These aggregates consist of fine prismatic deliensite crystals, reaching up to ~50 μm in length (Fig. 7).

The studied samples of deliensite from Abertamy and L'Ecarpière have been deposited in the collections of the Musée cantonal de géologie, Lausanne, Switzerland, under catalogue

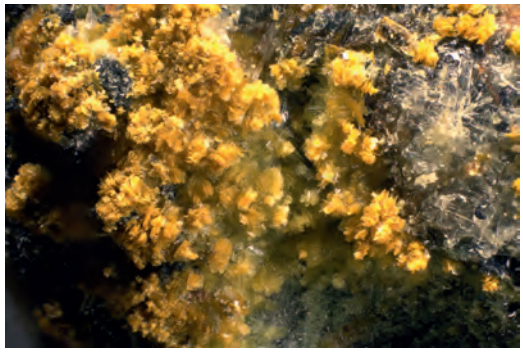

FIG. 5. Crystalline aggregate of deliensite crystals (orange to yellow orange) with gypsum (colourless) on altered uraninite (black or greyish black) from the Geister dump, Jáchymov ore district, Western Bohemia, Czech Republic. Field of view 3 mm (photo by P. Škácha).

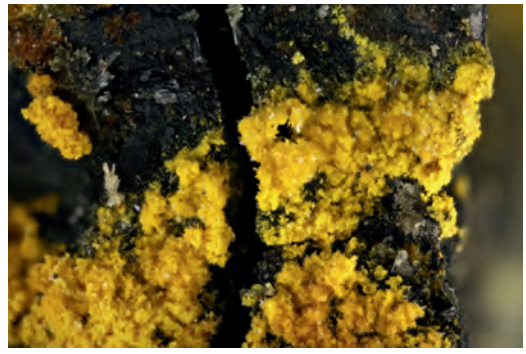

FIG. 6. Crystalline aggregates of deliensite with minor gypsum (colourless prismatic crystals in the left hand side of the picture) from L'Ecarpière mine, France on strongly altered blackish uraninite. Field of view 3 mm (photo by J.-M. Johannet).

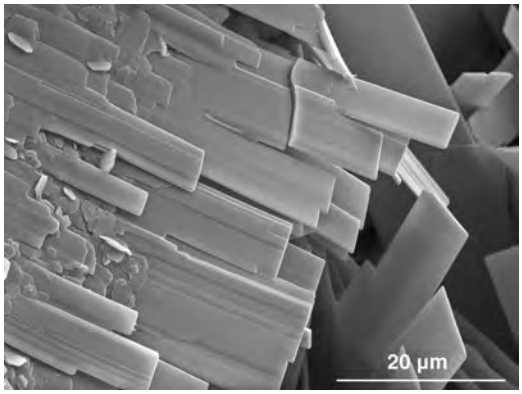

FIG. 7. Deliensite crystals from L'Ecarpière mine, France showing an apparently orthorhombic shape (image by N. Meisser).

numbers MGL 92633 and MGL 92634, respectively; the sample from Schweitzer has been catalogued in the collections of Museum Victoria, registration number M52018. Further specimens of deliensite from Jáchymov and Abertamy are held in the private collections of some of the authors and the sample from Lodève in the private collection of Jaroslav Hyršl.

Composition and scanning electron microscopy

Crystals from the deliensite specimen from Abertamy (which was used for structure determination), and from the L'Ecarpière specimen, were dissolved in a minute drop of 10% HCl, the addition of a small crystal of KSCN to the resulting solution produced no colouration for the Abertamy deliensite, but the solution from L'Ecarpière developed a strong blood-red colour due to formation of a $[Fe^{3+}(SCN)(H_2O)_5]^{2+}$ complex. A further examination by scanning electron microscopy showed that the deliensite was intimately intergrown with tiny (<5 μm) platy hexagonal crystals of copiapite, $Fe^{2+}Fe_4^{3+}(SO_4)_6(OH)_2{\cdot}20H_2O$. Semi-quantitative analysis by EDS suggested an atomic ratio Fe:U:S of ~1:2:2 for both samples (Abertamy and L'Ecarpière).

Quantitative analyses by WDS were undertaken on samples from the Mas d'Alary uranium deposit, Lodève; the Jeroným mine, Abertamy; and the Schweitzer and Geister mines in the Jáchymov district. Material from L'Ecarpière, France was also prepared for analysis but no deliensite crystals were found in the polished section (although another interesting phase was discovered and is described briefly in the following text). A Cameca SX100 electron microprobe operating in wavelength-dispersive spectrometry mode at an accelerating voltage of 15 kV, specimen current of 10 nA and 5 μm beam diameter was used. The X-ray lines and standards were selected to minimize overlaps and are as follows: $K\alpha$ lines: Al (sanidine), Si (sanidine), S (baryte), Ca (andradite), V (vanadinite), Fe (andradite), Mn (spessartine), Zn (ZnO); $L\alpha$ lines: Cu (dioptase), As (InAs); $M\alpha$ lines: Pb (vanadinite); $M\beta$ lines: U (metallic U). Peak counting times were 10–20 s; the counting time for background was 50% of the peak. Measured intensities were converted to elemental concentrations using the *PAP* program (Pouchou and Pichoir, 1985).

Secondary electron images showing the crystal morphology were acquired using a Mira Tescan FEG scanning electron microscope at the University of Lausanne.

The composition of deliensite from Mas d'Alary is listed in Table 1. The empirical formula, calculated from a mean of 7 analyses, and based on Fe + Al + Mg + U + S + Si + P + As = 5 atoms per formula unit (a.p.f.u.) is $(Fe_{0.82}Al_{0.06}Mg_{0.03})_{\Sigma 0.91}(UO_2)_{2.06}[(SO_4)_{1.89}(SiO_4)_{0.07}(PO_4)_{0.01}(AsO_4)_{0.01}]_{\Sigma 1.98}(OH)_{1.93}(H_2O)_7$. The only significant substitutions for Fe at the octahedral cation site are Al (at up to 0.1 a.p.f.u.) and Mg (at up to 0.04 a.p.f.u.).

The composition of the sample from the Jeroným mine, Abertamy is characterized by an increase in the proportion of M^{2+} cations at the octahedral site (Table 1). The empirical formula for the Abertamy sample (obtained from only one analysis due to problematic surface textures) is $(Fe_{0.58}Mg_{0.27}Zn_{0.16}Ca_{0.02})_{\Sigma 1.03}(UO_2)_{2.02}[(SO_4)_{1.88}(SiO_4)_{0.08}]_{\Sigma 1.96}(OH)_{2.00}(H_2O)_7$. It is interesting to note that although the Mg and Zn contents of the Abertamy sample are relatively high, no Mg- or Zn-dominant uranyl sulfates, with a U:S ratio 2:2 and a structure based on phosphuranylite topology are known.

Samples from Schweitzer and Geister mines in the Jáchymov district (Table 1) also have complex substitutions in the cation site. The empirical formula of the crystals from Schweitzer mine, calculated from a mean of the two listed analyses, and based on Fe + Zn + Mn + Al + U + S + Si + P + As = 5 a.p.f.u., is $(Fe_{0.78}Zn_{0.17}Mn_{0.03}Al_{0.02})_{\Sigma 1.00}(UO_2)_{2.10}[(SO_4)_{1.85}(SiO_4)_{0.02}(PO_4)_{0.02}(AsO_4)_{0.01}]_{\Sigma 1.90}(OH)_{2.40}(H_2O)_7$; for the Geister

TABLE 1. Composition of deliensite from various localities determined by wavelength-dispersive spectrometry.

	Mas d'Alary (seven analyses)			Jeroným mine, Abertamy (one analysis)	Schweitzer mine, Jáchymov (two analyses, which are listed below)			Geister mine, Jáchymov (one analysis)
	Mean	Range	SD		Mean	Anal. 10	Anal. 11	
Composition (wt.%)								
Al_2O_3	0.31	0.11–0.54	0.14		0.12	0.15	0.10	0.17
MgO	0.13	0.07–0.17		1.17				b.d.
CaO				0.11				0.15
MnO					0.23	0.17	0.29	0.14
ZnO				1.40	1.48	1.44	1.53	2.08
FeO	6.60	4.95–7.19	0.71	4.45	6.03	6.20	5.86	5.24
CuO								0.37
PbO								0.47
SiO_2	0.45	0.26–0.75	0.17	0.53	0.12	0.16	0.08	0.70
V_2O_5								0.19
P_2O_5	0.09	0.04–0.14	0.03		0.14	0.16	0.12	0.11
As_2O_5	0.13	0.15–0.25	0.10		0.12	0.15	0.10	0.24
SO_3	15.94	15.61–16.99	0.62	16.17	16.01	16.00	16.01	15.18
UO_3	61.90	59.10–64.24	1.93	62.18	64.92	64.08	65.77	63.56
H_2O*	15.13			15.52	15.95			15.73
Total	100.70	82.03–88.39		101.54	105.14	88.50	89.84	104.31
M-site cations per formula unit								
Al	0.057	0.019–0.104			0.022			0.031
Mg	0.030	0.018–0.040		0.270				–
Ca				0.018				0.024
Mn					0.030	0.022	0.038	0.018
Zn				0.160	0.169	0.164	0.174	0.235
Fe	0.816	0.674–0.919		0.576	0.777	0.800	0.755	0.672
Cu								0.042
Pb								0.020
Σ*M*-site	0.903	0.761–0.965		1.024	0.998	0.986	0.967	1.042

Anions per formula unit							
SiO_4	0.072	0.039–0.123	0.082	0.018	0.024	0.012	0.108
VO_4							0.019
PO_4	0.014	0.006–0.019		0.018	0.021	0.016	0.014
AsO_4	0.011	0.013–0.021		0.010	0.012	0.008	0.019
SO_4	1.892	1.851–1.998	1.876	1.852	1.855	1.850	1.748
ΣT-site	1.990	1.949–2.086	1.958	1.898	1.912	1.886	1.908
UO_2^{2+}	2.055	2.030–2.152	2.019	2.103	2.077	2.129	2.049
H_2O + OH	7.966	7.777–8.041	8.001	8.201	8.183	8.128	8.051

* Calculated from the ideal content of $7H_2O$ + 2OH in the crystal structure and for charge balance.

mine the empirical formula (calculated from only one analysis due to problematic surface textures) is $(Fe_{0.67}Zn_{0.24}Cu_{0.04}Al_{0.03}Mg_{0.02}Ca_{0.02}Pb_{0.02})_{\Sigma 1.04}(UO_2)_{2.05}[(SO_4)_{1.75}(SiO_4)_{0.11}(AsO_4)_{0.02}(VO_4)_{0.02}(PO_4)_{0.01}]_{\Sigma 1.91}(OH)_{2.10}(H_2O)_7$. Supergene vanadium minerals are more abundant in the Geister vein (Ondruš *et al.*, 1997).

Unidentified $Fe(UO_2)(SO_4)_2 \cdot nH_2O$

A currently unidentified phase was found on the specimen from L'Ecarpière mine, France (Table 2). Its empirical formula on the basis of 2 S + Si a.p.f.u. using a mean of 5 analyses is $(Fe_{0.71}Mg_{0.20}Zn_{0.08}Mn_{0.02})_{\Sigma 1.01}(UO_2)_{1.01}[(SO_4)_{1.98}(SiO_4)_{0.02}]_{\Sigma 2.00}(H_2O)_n$. A similar phase, with Fe:U:S in the ratio 1:1:2, is known from Lodève (Anatoly Kasatkin, pers. comm.). This potentially new mineral is currently under investigation by the authors.

Johannite

Johannite with an elevated Fe^{2+} content is present on the specimen from Abertamy. It is not easily distinguished from deliensite by optical microscopy, as it has a similar colour and habit. Its chemical composition (Table 2) corresponds to the empirical formula $(Cu_{0.52}Fe_{0.11}\square_{0.37})_{\Sigma 1.00}(UO_2)_{2.14}[(SO_4)_{2.12}(SiO_4)_{0.11}]_{\Sigma 2.23}(OH)_{0.91}(H_2O)_8$ (based on 2 S a.p.f.u. and a mean of three analyses).

Thermal analysis

Thermal analysis of deliensite was carried out using a Stanton Redcroft TG 750 Thermobalance at a heating rate of 10ºC min^{-1} and a dynamic air flow rate of 25 ml min^{-1}. The extremely low sample mass (0.018 mg), relatively high gas-flow rate, and partly overlapping decomposition steps, resulted in shifts of the thermogravimetric curve to higher temperatures than expected in comparison with the thermal decomposition of natural and synthetic johannite (Čejka *et al.*, 1988; Sokol and Čejka, 1992). Therefore, only tentative assignments of the temperatures of each partly overlapping decomposition step could be made; these are as follows: ~4 H_2O (~365ºC); ~1.5 H_2O (~470ºC); ~1.5 H_2O + ~1 H_2O ($2OH^-$) + ~1 SO_3 (650ºC); ~1 SO_3 + ~0.33 O_2 (~865ºC). The total mass loss is approximately 8 H_2O (7 H_2O + 2 OH^-) + ~2 SO_3 + ~0.33 O_2, which is consistent

TABLE 2. Composition of minerals associated with deliensite, determined by wavelength-dispersive spectrometry.

	Unnamed phase, L'Ecarpière, France (mean of five analyses)			Johannite-like phase, Jeroným mine, Abertamy (mean of three analyses)		
	Mean	Range	SD	Mean	Range	SD
Composition (wt.%)						
Al_2O_3						
MgO	1.34	1.22–1.49	0.08			
CaO						
MnO	0.17	0.12–0.27	0.06			
ZnO	1.05	1.02–1.09	0.04			
FeO	8.41	7.91–9.36	0.62	0.88	0.49–1.14	0.34
CuO				4.60	4.27–4.87	0.30
PbO						
SiO_2	0.16	0.08–0.23	0.06	0.70	0.59–0.89	0.17
V_2O_5						
P_2O_5					0.14	0.16
As_2O_5					0.12	0.15
SO_3	26.17	25.10–26.80	0.71	18.69	17.97–19.47	0.75
UO_3	47.68	45.87–48.70	1.13	67.68	66.40–69.02	1.31
H_2O				16.81*	15.95	
Total				109.35		
Cations per formula unit						
Al						
Mg	0.201	0.187–0.217				
Ca						
Mn	0.015	0.010–0.023				
Zn	0.079	0.076–0.083				
Fe	0.710	0.667–0.770		0.111	0.061–0.143	
Cu				0.524	0.498–0.548	
Pb						
Σ*M*-site	1.005	0.940–1.093		0.635	0.569–0.691	
Anions per formula unit						
SiO_4	0.017	0.008–0.024		0.106	0.083–0.137	
VO_4						
PO_4						
AsO_4						
SO_4	1.983	1.976–1.992		2.115	2.082–2.177	
Σ*T*-site	2.000			2.121		
UO_2^{2+}	1.012	0.948–1.074		2.144	2.116–2.164	
H_2O + OH				8.454		

* Calculated on the base of the ideal content of 8 H_2O in the structure of johannite with the OH content derived from charge balance.

with the H_2O content obtained from the structure refinement.

On the basis of their analysis of the thermogravimetric curve of deliensite (heating rate 5ºC min^{-1}, N_2-flow 50 ml min^{-1}) Vochten *et al.* (1997) reported that dehydration and dehydroxylation do not take place in distinct steps and occur between 110 and 500ºC and that decomposition of the sulfate group occurs between 500 and 800ºC.

Infrared and Raman spectroscopy

Infrared spectra of the deliensite samples were collected on a Nicolet Magna 760 FTIR spectrometer in the spectral range 4000–600 cm^{-1}, at a

resolution of 4 cm^{-1}, using an average of 128 scans and Happ–Genzel apodization. The spectrometer was equipped with a Spectra Tech InspectIR micro-FTIR accessory and operated using the DRIFTS method. A small amount of the sample was powdered, mixed with KBr, and analysed immediately. The same KBr was used as a reference. Raman spectra of samples from the Jeroným mine, Abertamy and the Schweitzer mine, Jáchymov, were collected using a DXR dispersive Raman spectrometer (Thermo Scientific) on a confocal Olympus microscope with a 100× objective in the range 50–6400 cm^{-1} at a spectral resolution of 2 cm^{-1}. The experimental parameters were as follows: excitation wavelength, 532 nm; exposure time, 10 s; number of exposures, 32; grating, 400 lines per mm; spectrograph aperture, 50 μm slit; camera temperature, 50ºC; laser power, 3.0 mW; and CCD detector. Spectra were processed (background correction and peak fitting) using *OMNIC Spectral tool* v.7.3 (ThermoElectron). The assignments of the infrared and Raman bands in the spectrum of deliensite are based on the relatively limited amount of available data for sulfate minerals (Nakamoto, 1986; Lane, 2007), and especially uranyl sulfates (Čejka, 1999, 2004, 2007 and references therein). The T_d symmetry of the free $(SO_4)^{2-}$ anion is typically reduced to C_{2v} or less due to the bond interactions. The doubly degenerate ν_2 (δ) $(SO_4)^{2-}$ bending vibration, the triply degenerate ν_3 $(SO_4)^{2-}$ antisymmetric stretching vibration, and the ν_4 (δ) $(SO_4)^{2-}$ bending vibration therefore split. All 'daughter' vibrations may be Raman and infrared active. For the sample from the Schweitzer mine at Jáchymov, both infrared and Raman spectra were acquired. For the sample from Jeroným mine, Abertamy, only the Raman spectrum was collected.

Vibrational spectroscopy of OH^- and H_2O groups

The Raman bands in the highest wavenumber region shown in Fig. 8, ~6300 cm^{-1}, correspond to the first overtones of ν O–H vibrations of H_2O groups. These bands are similar to those observed in the near infrared spectra of other uranyl minerals (e.g. Frost and Čejka, 2009). Infrared and Raman bands and shoulders between 3500 and 3100 cm^{-1} (shown in detail in Fig. 9) are attributed to the ν O–H stretching vibrations of structurally distinct hydrogen bonded H_2O molecules and hydroxyl ions. According to the empirical relation of Libowitzky (1999), the O–H···O hydrogen-bond lengths are in the

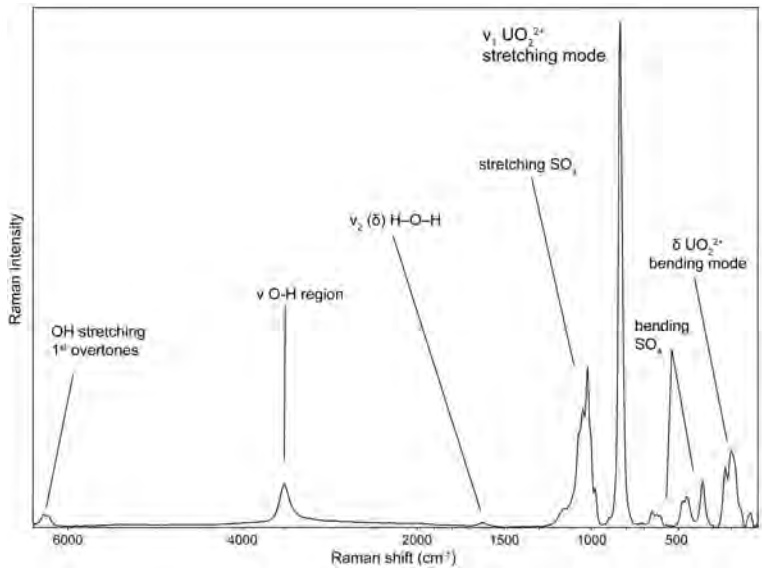

FIG. 8. Raman spectrum of deliensite from the Schweitzer dump, Jáchymov ore district, Western Bohemia, Czech Republic showing band assignments.

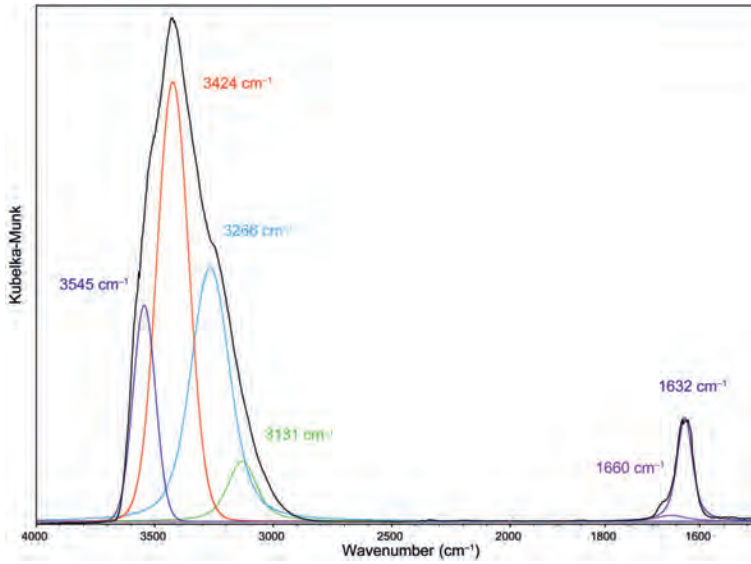

FIG. 9. Best fits to the O–H stretching vibrations in the infrared spectrum of deliensite from the Schweitzer dump, Jáchymov ore district, Western Bohemia, Czech Republic.

approximate range 2.69 to 2.99 Å. Corresponding separation distances between appropriate oxygen atoms were confirmed in the crystal structure refinement. Weak Raman bands and shoulders at ~1620 and 1640 cm^{-1} (Fig. 8) and infrared bands and shoulders at 1632 and 1660 cm^{-1} (Fig. 9) are assigned to the ν_2 (δ) bending vibrations of structurally distinct H_2O groups. The tentative assignment of some of the weak bands or shoulders in the range 933 to 722 cm^{-1} to δ U–OH and γ U–OH bending vibrations is problematic due to overlap with $(UO_2)^{2+}$ stretching vibrations. Some of the weak bands in this region may be also related to the libration modes of H_2O. Moreover, an overlap of the bands at ~980 cm^{-1} (Raman), and 978 cm^{-1} (infrared) with the ν_1 $(SO_4)^{2-}$ symmetric stretching vibrations is also possible.

Vibrational spectroscopy of $(SO_4)^{2-}$

Infrared bands with shoulders between ~1200 and 1060 cm^{-1} (Fig. 10) and Raman bands at ~1200 to 1050 cm^{-1} (Fig. 8), respectively, are attributed to split ν_3 $(SO_4)^{2-}$ antisymmetric stretching vibrations. Those between ~1000 and 1030 cm^{-1} (infrared and Raman) correspond to the ν_1 $(SO_4)^{2-}$ symmetric stretching vibration. The number of these vibrations is due to multiplication of the sulfur atoms in the primitive spectroscopic unit cell of deliensite. Raman bands and shoulders between 660 and 600 cm^{-1} are assigned to split ν_4 (δ) $(SO_4)^{2-}$ bending vibrations and those between 490 and 440 cm^{-1} to split ν_2 (δ) $(SO_4)^{2-}$ bending vibrations (Fig. 8).

Vibrational spectroscopy of $(UO_2)^{2+}$

The very weak infrared band at ~840 cm^{-1} (Fig. 10) and the very strong Raman band at 838 cm^{-1} (with shoulders at 824 and 853 cm^{-1}) for the sample from the Schweitzer mine, Jáchymov (Fig. 8) and at 840 cm^{-1} (with shoulders at 830 and 849 cm^{-1}) for the sample from the Jeroným mine, Abertamy are assigned to the ν_1 $(UO_2)^{2+}$ symmetric stretching vibration. The medium-strong infrared bands at 933 cm^{-1} (with a shoulder at 915 cm^{-1}) and the very weak Raman bands at 901 cm^{-1} (Schweitzer) (Fig. 8) and 897 cm^{-1} (Abertamy) are assigned to the ν_3 $(UO_2)^{2+}$ antisymmetric stretching vibration. According to the data of Bartlett and Cooney (1989), the approximate U–O bond length in the uranyl ion inferred from the positions of the observed infrared and Raman bands is in the range 1.76–1.79 Å. These values are in agreement with those reported by Burns *et al.* (1997) for uranyl pentagonal bipyramids. Raman bands and shoulders at ~360 cm^{-1} are associated with ν $(U–O_{ligand})$ stretching vibrations. Those at

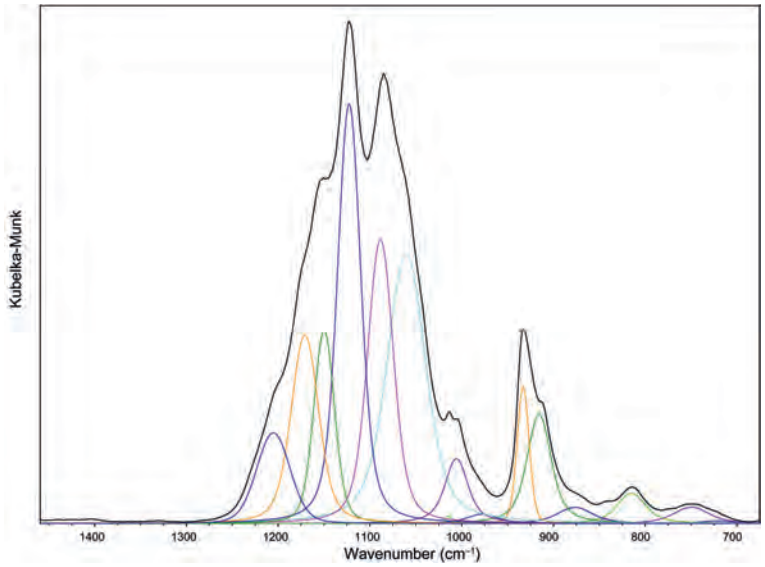

FIG. 10. Best fits to the fundamental $(SO_4)^{2-}$ and $(UO_2)^{2+}$ vibrations in the infrared spectrum of deliensite from the Schweitzer dump, Jáchymov ore district, Western Bohemia, Czech Republic.

~240 cm^{-1} are assigned to split ν_2 (δ) $(UO_2)^{2+}$ bending vibrations. Raman bands and shoulders at the lowest wavenumbers are attributed to lattice modes.

Crystal structure of deliensite

Experimental

A $0.11 \times 0.03 \times 0.01$ mm colourless prismatic crystal of deliensite from the Jeroným mine, Abertamy was selected for study by single-crystal X-ray diffraction on an Oxford diffraction SuperNova diffractometer with an EoS CCD detector and Mo*K*α (λ = 0.71073 Å) radiation monochromated using primary mirror optics. The unit cell was refined from 3629 reflections using *CrysAlis* software (Agilent Technologies) to give an orthorhombic unit cell with a = 15.8514(9), b = 16.2478(7), c = 6.8943(3) Å, V = 1775.63(12) $Å^3$ and Z = 4. Some unindexed reflections were found to be the result of non-merohedral rotational twinning (Fig. 11), in which the second twin component is related to the first one by the following twinning matrix: (−1, 0.073, 0/ 0.0694, 1, 0/ 0, 0, −1). At a later stage of the refinement it was found that the dataset also included reflections arising from inversion twinning. For data reduction within the *CrysAlis RED* routine, an *hklf5* procedure was used. A total of 8853 reflections were measured, with 5211 being classified as uniquely observed [$I_{obs} > 3\sigma(I)$]. Although other approaches based on partial data sets for each domain were tried, the *hklf5* procedure provided the best results. An empirical absorption correction was applied (multi-scan, *ABSPACK*, Agilent Technologies) and resulted in an agreement index, R_{int}, of 0.0947. A summary of the data collection, crystallographic data and refinement is given in Table 3.

A single $0.03 \times 0.03 \times 0.01$ mm crystal from the Schweitzer mine, Jáchymov was investigated on the MX2 beamline at the Australian Synchrotron, Melbourne, Victoria, Australia. Refined unit-cell parameters are listed in Table 4. The crystal structure refined to R_1 = 0.1080 and the results are consistent with those obtained from the Abertamy sample; however, due to the quality of the crystal only isotropic atomic-displacement parameters could be refined. As a result, only the Abertamy refinement is discussed in detail. A crystallographic information file has been deposited with *Mineralogical Magazine* and is available at http://www.minersoc.org/pages/e_journals/dep_mat_mm.html.

A crystal of deliensite from the type locality, Mas d'Alary, Lodève, France was examined using an Oxford diffraction Gemini single-crystal diffractometer system equipped with an Atlas detector (using monochromatic Mo*K*α radiation) and a fibre-optic Mo-Enhance collimator. The

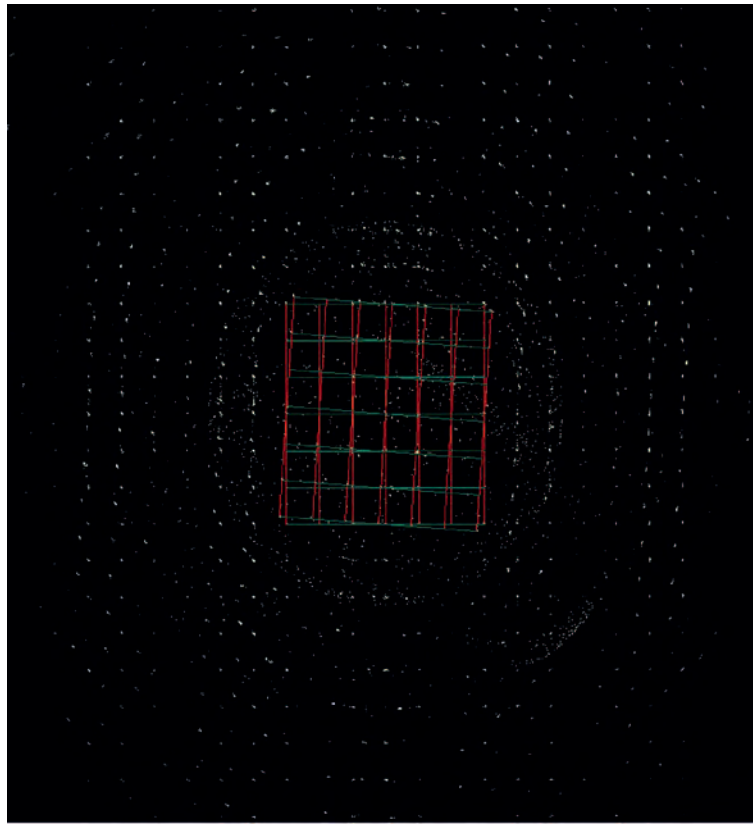

FIG. 11. Reciprocal space reconstruction from the experimental dataset, viewed along **c***, showing two rotational twin domains.

quality of the crystal did not allow for a full structure solution. The unit-cell parameters were refined using the least-squares algorithm in *CrysAlis* from 107 reflections (from 8.01–1.06 Å) and are listed in Table 4.

Structure solution and refinement

The crystal structure of deliensite (Table 5) was solved using the charge-flipping algorithm (Palatinus and Chapuis, 2007) and subsequently refined using *Jana2006* software (Petříček *et al.*, 2006). The reflection conditions clearly indicated a *P*-lattice with *n*-glides on *a* and *b*, suggesting two possible space groups: *Pnnm* and *Pnn*2. No cell of higher symmetry was found using the *Platon ADDSYMM* program (Spek, 1988, 2003, 2009). Subsequent refinements were performed for both structure models, with disordered (centrosymmetric *Pnnm*) and ordered (non-centrosymmetric *Pnn*2) models. The ordered model also involves an inversion (merohedral) twin, as suggested by the Flack parameter of 0.47(4), and Hooft parameter of 0.507(7) (*PLATON* program; Hooft *et al.*, 2008). Two and four twinning matrices describing the twin domains for the centrosymmetric and non-centrosymmetric models were used in refinements in *Jana2006*. Significantly poorer *R*-indices were produced by the centrosymmetric model (R_{obs} ~ 0.10), compared to the non-centrosymmetric model.

All atoms, except U and Fe, were refined isotropically. Some anisotropic atomic-displacement parameters (ADPs) refined to unrealistically small values, therefore some atoms had to be constrained to have equal ADPs (e.g. the oxygen atoms in the sulfate tetrahedra). Problems with ADPs may be ascribed to inappropriately corrected absorption effects as well as twinning.

TABLE 3. Summary of data collection conditions and refinement parameters for deliensite from the Jeroným mine, Abertamy.

Ideal structural formula	$Fe[(UO_2)_2(SO_4)_2(OH)_2](H_2O)_7$
Unit-cell parameters (based on 3999 reflections)	
a	15.8474(7) Å
b	16.2530(7) Å
c	6.8938(1) Å
V	1775.6(1) Å^3
Z	4
Temperature	293 K
Radiation, wavelength	Mo*K*α, 0.71073 Å
Crystal dimensions	0.11 × 0.03 × 0.01 mm
Collection mode, frame width, count time	ω scans to fill Ewald sphere, 0.5º, 90 s
limiting θ angles	1.788º–28.174º
limiting Miller indices	$-20 < h < 21$, $-20 < k < 19$, $-9 < l < 9$
No. of reflections measured	9210
No. of unique reflections	8853
No. of observed reflections [criterion]	5211 [I_{obs}>3σ(I)]
R_{int}	0.0947
Absorption correction, method	19.198mm^{-1}, multi-scan
F_{000}	1640
Refinement details (*Jana2006* on *F*)	
Space group	*Pnn*2
Parameters refined, restraints, constraints	118, 2, 7
R_{obs}, wR_{obs}	0.0624, 0.0604
R_{all}, wR_{all}	0.1030, 0.0630
GOF obs/all	2.35/1.87
$\Delta\rho_{min}$, $\Delta\rho_{max}$	−3.86, 8.64 e Å^{-3} (close to U1)
Twin components* Tw_{vol1}/Tw_{vol2}; Tw_{vol3}/Tw_{vol4}	0.25(2)/0.24(1); 0.23(2)/0.29(1)
Weighting scheme, weights	σ, $w = 1/(\sigma^2(F) + 0.0001F^2)$

* The abbreviations Tw_{vol1}/Tw_{vol2} indicate the non-merohedral twin domains; Tw_{vol3}/Tw_{vol4} indicate the inversion twins.

TABLE 4. Refined unit-cell parameters for deliensite from four localities.

	1	2	3	4	5	6	7
a	15.8489(10)	15.86(2)	15.877(3)	15.865(5)	15.84(1)	15.908(5)	15.85(1)
b	16.2509(7)	16.30(2)	16.279(3)	16.278(6)	16.27(2)	16.274(3)	16.34(3)
c	6.8928(3)	6.92(1)	6.9000(13)	6.908(3)	6.889(6)	6.903(1)	6.907(8)
V	1775.29(10)	1787(4)	1783.4(6)	1784(1)	1775(3)	1787(1)	1790(3)

1. Jeroným mine, Abertamy, Czech Republic; single crystal diffraction; this study.
2. Jeroným mine, Abertamy, Czech Republic; powder diffraction; this study.
3. Schweitzer mine, Jáchymov, Czech Republic; synchrotron single crystal diffraction; this study.
4. Schweitzer mine, Jáchymov, Czech Republic; powder diffraction; this study.
5. Mas d'Alary, Lodève, France; single crystal diffraction; this study.
6. Mas d'Alary, Lodève, France; powder diffraction; Vochten *et al*. (1997).
7. L'Ecarpière, France; powder diffraction; this study.

TABLE 5. Atom positions and displacement parameters (Å^2) for Abertamy deliensite.

Atom	a/x	b/y	c/z	U_{iso}/U_{eq}	U_{11}	U_{22}	U_{33}	U_{12}	U_{13}	U_{23}
U1	0.28494(4)	0.29041(3)	0.012550(3)	0.0112(2)	0.0202(3)	0.0083(3)	0.0052(2)	−0.0010(3)	−0.0060(9)	−0.004(1)
U2	0.29072(5)	0.05284(3)	0.010290(3)	0.0139(2)	0.0278(4)	0.0076(3)	0.0064(2)	0.0002(3)	0.003(1)	−0.003(1)
S1	0.2358(2)	0.3330(2)	0.50649(2)	0.0116(7)						
S2	0.2444(2)	0.0086(2)	0.51334(2)	0.0145(8)						
Fe*	0.0313(1)	0.3099(1)	0.000000(7)	0.0158(7)	0.019(1)	0.021(2)	0.007(1)	−0.002(1)	−0.002(2)	0.006(3)
O1	0.1784(5)	0.3012(5)	0.00789(8)	0.012(1)						
O2	0.1848(6)	0.0363(5)	0.01462(8)	0.021(2)						
O3	0.4023(6)	0.0640(5)	0.00972(8)	0.021(2)						
O4	0.1835(5)	0.2568(5)	0.50583(8)	0.010(2)						
O5	0.1791(5)	0.4028(5)	0.48903(8)	0.015(2)						
O6	0.3005(9)	0.338(1)	0.34101(8)	0.019(5)						
O7	0.2081(8)	0.5022(9)	0.18478(8)	0.008(1)						
O8	0.3108(8)	0.0103(9)	0.34383(8)	0.008(1)						
O9	0.2009(5)	0.0883(5)	0.50838(8)	0.008(1)						
O10	0.3095(5)	0.4309(5)	0.00030(8)	0.008(1)						
O11	0.3887(5)	0.2809(5)	0.00812(8)	0.012(2)						
O12	0.2866(8)	0.174(1)	0.20460(8)	0.007(1)						
O13	0.2339(7)	0.673(1)	0.32240(8)	0.007(1)						
O14	0.2843(8)	0.336(1)	0.68480(8)	0.002(3)						
O15	0.4001(5)	0.1773(6)	0.51124(8)	0.024(2)						
O16	0.5417(9)	0.0702(9)	0.38544(8)	0.045(4)						
O17	0.5378(9)	0.2366(9)	0.23119(8)	0.036(4)						
O18	0.0282(1)	0.1852(9)	0.10716(8)	0.046(4)						
O19	0.0358(8)	0.3546(8)	0.29215(8)	0.033(4)						
O20	0.465(1)	0.420(1)	0.33372(8)	0.052(5)						
O21	0.024(1)	0.087(1)	0.41914(8)	0.075(6)						

* Site occupancy of Fe atom is 0.93(1).

The final cycle of the refinement converged to R_{obs} = 0.0624, R_{all} = 0.1030 and wR_{all} = 0.0630 with a GOF_{all} = 1.87. The atom positions and displacement parameters are listed in Table 5. Geometrical information and a bond-valence analysis are included in Tables 6 and 7, respectively. The bond-valence analysis was carried out following the procedure of Brown (1981, 2002). The bond-valence sums (Table 7) are in accordance with the expected valence states of the elements present and helped in the assignment of OH and H_2O. All of the significant difference-Fourier maxima are located in the vicinity of the uranium atoms and are probably connected with the unresolved twinning features and inappropriately corrected absorption.

Description of the crystal structure

There are two unique U sites in the structure of deliensite. Each U atom is strongly bonded to two apical oxygen atoms, forming a uranyl ion $(UO_2)^{2+}$. The mean bond lengths, <U1–O> and <U2–O>, are 1.68 and 1.75 Å, respectively. These distances are smaller than the average reported for U^{6+} compounds of ~1.8 Å (Burns, 2005; Burns *et al.*, 1997). Uranium atoms are further coordinated by five ligands, including O and OH^-, arranged at the equatorial apices of uranyl pentagonal bipyramids capped by uranyl oxygen atoms at the vertices. These bipyramids form edge-sharing dimers; both oxygen atoms at the shared edges belong to OH groups. There are two unique S atom sites, both of which are in tetrahedrally coordinated $(SO_4)^{2-}$ groups. The uranyl dimers are linked by sharing vertices with the sulfate tetrahedra to form sheets perpendicular to (010) (Fig. 9). These structural sheets, which can be described as being made of $[(UO_2)_2(SO_4)_2(OH)_2]^{2-}$, are also present in the mineral phosphuranylite (Burns, 2005).

There is one unique Fe site which is coordinated by six ligands, including one O atom of the structural sheet (O_{Ur}) and five H_2O groups in a slightly distorted octahedral arrangement (Table 6). In the interlayer there are an additional two O atoms in weakly bonded molecular H_2O (Table 7). Adjacent uranyl

TABLE 6. Selected interatomic distances (Å) and geometrical parameters for deliensite from the Jeroným mine, Abertamy.

U1–O1	1.698(8)	U2–O2	1.701(9)
U1–O11	1.653(8)	U2–O3	1.778(9)
U1–O6	2.407(6)	U2–O5	2.489(9)
U1–O10	2.317(8)	U2–O7	2.390(5)
U1–O12	2.312(13)	U2–O8	2.422(4)
U1–O13	2.332(14)	U2–O12	2.379(13)
U1–O14	2.377(5)	U2–O13	2.377(14)
<U–O_{Ur}>	**1.68**	**<U–O_{Ur}>**	**1.74**
<U–O_{eq}>	**2.35**	**<U–O_{eq}>**	**2.41**
S1–O4	1.490(9)	S2–O7	1.405(7)
S1–O5	1.452(10)	S2–O8	1.573(8)
S1–O6	1.535(10)	S2–O9	1.468(9)
S1–O14	1.450(7)	S2–O10	1.527(9)
<S1–O>	**1.48**	**<S2–O>**	**1.49**
Fe–O1	2.337(8)		
Fe–O15	2.092(8)	*V*	13.010 Å^3
Fe–O16	2.108(14)	Δ	0.034
Fe–O17	2.004(6)	σ^2	8.41
Fe–O18	2.157(14)	ECoN	5.47
Fe–O19	2.142(5)		
<Fe–O>	**2.14**		

Symbols used are as follows: Δ, bond-length distortion after Brown and Shannon (1973); σ^2, bond-angle distortion after Robinson *et al.* (1971); ECoN, effective coordination number after Hoppe (1979).

TABLE 7. Bond-valence analysis for deliensite from the Jeroným mine, Abertamy.

	U1	U2	Fe	S1	S2	ΣBV	Assignment
O1	1.97		0.20			2.17	O
O2		1.96				1.96	O
O3		1.69				1.69	O
O4				1.44		1.44	O
O5		0.42		1.59		2.01	O
O6	0.49			1.27		1.76	O
O7		0.51			1.81	2.32	O
O8		0.48			1.15	1.63	O
O9					1.52	1.52	O
O10	0.59				1.30	1.89	O
O11	2.16					2.16	O
O12	0.59	0.52				1.11	OH
O13	0.57	0.52				1.09	OH
O14	0.52			1.60		2.12	O
O15			0.38			0.38	H_2O
O16			0.36			0.36	H_2O
O17			0.48			0.48	H_2O
O18			0.32			0.32	H_2O
O19			0.33			0.33	H_2O
O20						0.00	H_2O
O21						0.00	H_2O
	6.89	6.10	2.07	5.90	5.78		

Values are expressed in valence units (vu).
The U^{6+}–O bond strengths (r_0 = 2.045, b = 0.51) are from Burns *et al.* (1997); S^{6+}–O and Fe^{2+}–O bond strengths are from Brown and Altermatt (1985).

sulfate structural sheets are only linked by hydrogen bonds; the $FeO(H_2O)_5$ octahedra are non-bridging (Fig. 12). The weak interaction between the layers (interplanar distance ~7.94 Å) produces the excellent cleavage of deliensite and is also obvious in the powder diffraction pattern [i.e. calculated d_{200} 7.925 Å (rel. int. 100), reported by Vochten *et al.* (1997) cf. d_{obs} = 7.94 (rel. int. 100) (Table 8)].

Powder X-ray diffraction

Powder X-ray diffraction patterns of deliensite were obtained using two systems. A Bruker D8 Advance diffractometer with a LynxEye detector using Cu*K*α radiation was used for sample JACH246. Data were collected at a step size of 0.01° with variable counting times (total counting time 48 h). Due to the small amount of material available from the L'Ecarpière mine, France and Jeroným mine, Abertamy, a 114.6 mm Gandolfi camera operating at 40 kV and 30 mA and using Ni-filtered Cu*K*α radiation with 100 h exposure time was used. Elemental Si was used as an external standard and intensities were visually estimated. For the least-squares unit-cell refinement, the non-linear least squares algorithm in the *Unitcell* program (Holland and Redfern, 1997) was used. Refined unit-cell parameters are listed in the Table 4. Indexed powder diffraction patterns are listed in Table 8.

Discussion

Original description of deliensite and relationship to the other uranyl sulfates

Deliensite was described as a new mineral with an ideal formula $Fe(UO_2)_2(SO_4)_2(OH)_2(H_2O)_3$ from the Mas d'Alary uranium deposit, Lodève, France (Vochten *et al.*, 1997). On the basis of a Weissenberg film analysis the orthorhombic space groups *Pnnm* or *Pnn*2 were reported, with unit-cell parameters a = 15.908(5), b = 16.274(3), c = 6.903(l) Å^3, V = 1787(l) Å and Z = 4. Vochten *et al.* (1997) calculated the water content in their ideal formula based on a thermogravimetric study

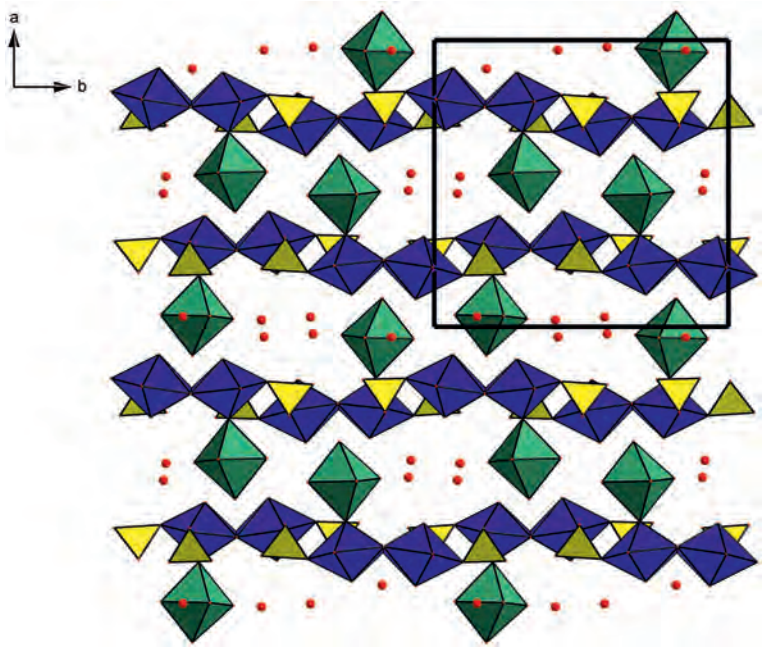

FIG. 12. Crystal structure of deliensite viewed along [001]. Structural sheets consisting of uranyl pentagonal bipyramids (blue) and sulfate tetrahedra (yellow) are separated by an interlayer containing iron-centred octahedra (green) and H_2O (oxygen atoms, red). The edges of the unit cell are outlined.

which revealed a total weight loss of 8.63% (to 250ºC). This was assigned to a release of H_2O from the structure, corresponding to 2.082 OH and 3.179 H_2O. This method can be called into question as the release of OH bonded to structural sheets is likely to take place at temperatures higher than 250ºC (e.g. Čejka *et al.*, 1988; Sokol and Čejka, 1992). Moreover, the content of three H_2O molecules per Fe in the formula is, for crystal-chemical reasons, more unlikely than, for example, four H_2O molecules; in latter case Fe would be expected to act as a bridge between adjacent layers. It is probable that insufficient material was available on the type specimen for a definitive thermogravimetric study, and that the reported mass loss to 250ºC is only a fraction of the full amount.

A few other compounds contain sheets with the same uranyl-anion topology as deliensite (Table 9). They contain a structural sheet with the same composition but with important differences in the interlayer components (organically templated synthetic compounds and compounds with fluorine instead of OH on the sheets are not discussed here). In deliensite, Fe^{2+} does not act as a bridge linking adjacent uranyl-sulfate sheets as Cu^{2+} does in johannite (Fig. 13*a*). It has a different function from the Sr^{2+} cations which form [9]-coordinate edge-sharing $Sr_2\Phi_{16}$ dimers (Fig. 13*b*) in $Sr[(UO_2)_2(CrO_4)_2(OH)_2](H_2O)_8$. In synthetic $Mg(H_2O)_6[(UO_2)_2(CrO_4)_2(OH)_2](H_2O)_3$, there is one symmetrically unique [6]-coordinate interlayer Mg^{2+}, which does not link to either of the directly adjacent sheets (Fig. 13*c*) and two H_2O molecules held by hydrogen bonds only. The synthetic uranyl chromate, $Co(H_2O)_4(Co(H_2O)_6)_2[(UO_2)_4(CrO_4)_6(OH)_2](H_2O)_4$, has a complex interlayer containing two symmetrically distinct [6]-coordinate Co^{2+} cation sites. One occurs as an isolated octahedron and is held by hydrogen bonds only; two more symmetrically equivalent Co octahedra are linked by vertex sharing to sulfate tetrahedra in the uranyl-sulfate sheet (Fig. 13*d*). In johannite there are four transformer H_2O groups bonded to the Cu^{2+} cation and an additional four non-transformer H_2O groups, which are required to transfer the bond-valence from the interlayer cation to the anions in the sheets (Mereiter, 1982). In synthetic $Mg(H_2O)_6[(UO_2)_2(CrO_4)_2(OH)_2](H_2O)_3$, six transformer H_2O groups are coordinated to Mg. To propagate

TABLE 8. Powder X-ray diffraction data for deliensite samples.

	Schweitzer mine, Jáchymov, Czech Republic This study (JACH246)			L'Escarpière, Gétigné, France This study (NM 4405)			Jeroným mine, Abertamy, Czech Republic This study (NM 4406)		
h k l	d_{obs} (Å)	d_{calc} (Å)	I_{obs}	d_{obs} (Å)	d_{calc} (Å)	I_{obs}	d_{obs} (Å)	d_{calc} (Å)	I_{obs}
2 0 0	7.940	7.933	100	7.94	7.93	80	8.01	7.93	100
1 2 0	7.287	7.287	0.13	7.17	7.26	20	7.20	7.25	10
2 1 0	7.132	7.132	0.37						
0 1 1	6.356	6.359	0.02	6.37	6.36	30	6.37	6.37	20
1 1 1	5.901	5.903	0.26	5.91	5.90	100	5.93	5.91	100
2 2 0	5.660	5.681	0.03						
–				5.23*		5			
–				4.67*		5	4.68*		10
2 2 1	4.391	4.388	0.29						
0 3 1	4.269	4.267	0.06	4.27	4.28	30	4.26	4.27	30
3 0 1	4.198	4.199	0.25	4.17	4.20	30			
3 1 1	4.069	4.066	0.11						
4 0 0	3.965	3.966	20.5	3.96	3.92	100	3.95	3.97	80
4 1 0	3.856	3.854	0.97						
3 3 0	3.788	3.787	0.14	3.77	3.79	40	3.77	3.79	10
4 2 0	3.554	3.565	0.18						
0 0 2	3.452	3.454	0.30	3.45	3.45	80	3.46	3.46	70
3 4 0	3.227	3.225	0.18	3.23	3.23	50	3.21	3.23	30
2 4 1	3.203	3.207	0.09						
2 0 2	3.165	3.167	0.15	3.153	3.166	50	3.181	3.171	30
2 5 0	3.002	3.011	0.05						
0 5 1	2.950	2.945	0.07	2.964	2.955	40	2.954	2.948	20
1 5 1	2.896	2.896	0.05	2.917	2.905	10	2.898	2.898	20
5 0 1	2.883	2.883	0.15						
5 3 0	2.740	2.739	0.08	2.763	2.740	30	2.763	2.739	20
1 4 2	2.605	2.598	0.20	2.603	2.602	80	2.607	2.601	80
3 5 1	2.576	2.573	0.09						
4 1 2	2.576	2.272	0.09						
3 4 2	2.3568	2.3573	0.02	2.359		30	2.365	2.360	30
3 6 1				2.279	2.285	10			
1 1 3	2.2555	2.2568	0.03	2.259	2.257	10	2.257	2.260	20
4 4 2				2.191	2.196	5			
7 0 1	2.1541	2.1535	0.10	2.176	2.166	5			
4 6 1				2.120	2.135	20	2.120	2.131	50
6 4 1				2.108	2.112	20			
2 3 3	2.0464	2.0479	0.06	2.042	2.049	30			
0 8 0	2.0375	2.0348	0.06						
4 5 2	2.0375	2.0339	0.06						
8 0 0	1.9837	1.9832	0.17	1.993		10			
2 8 0	1.9685	1.9710	0.40						
8 1 0	1.9685	1.9686	0.40						
2 4 3				1.949	1.945	10			
0 5 3				1.886	1.882	20	1.881	1.883	20
3 8 1				1.838	1.837	20			
4 4 3				1.789	1.790	20	1.791	1.791	10
0 8 2				1.759	1.758	30	1.759	1.755	10
0 9 1	1.7482	1.7497	0.02						
0 0 4	1.7261	1.7270	0.04	1.725	1.727	30	1.728	1.730	10
8 4 1	1.7261	1.7262	0.04						
10 0 0	1.5861	1.5865	0.07	1.581	1.585	40	1.585	1.586	20

The differences in observed intensities between these datasets is due to the different collection geometries used to obtain the powder data (see text). The left hand column intensities show the effect of preferred orientation.
* Probably due to an admixed phase.

TABLE 9. Compounds containing dimers of edge-sharing uranyl pentagonal bipyramids linked through tetrahedral oxyanions based on phosphuranylite ($6^1 5^2 4^2 3^2$) topology with vacant hexagons.

Formula	Mineral	Space group	TO_4 orientation	Reference
$Fe[(UO_2)_2(OH)_2(SO_4)_2](H_2O)_7$	Deliensite	$Pnn2$	ddudd, uuduu	This study
$Cu[(UO_2)_2(OH)_2(SO_4)_2](H_2O)_8$	Johannite	$P\bar{1}$	ududud	Mereiter (1982)
$Sr[(UO_2)(OH)(CrO_4)](H_2O)_8$		$P\bar{1}$	ududud	Serezhkin *et al.* (1982)
$[C(NH_2)_3][(UO_2)(OH)(MoO_4)]$		$P2_1/c$	ududud	Halasyamani *et al.* (1999)
$(UO_2)_3(MoO_4)_2(OH)_2(H_2O)_{10}$		$Pbca$	uuuudd, dddduu	Tali *et al.* (1994)
$[N_2C_6H_{16}][UO_2F(SO_4)]_2$		$Pmmn$	ddudd, uuduu	Doran *et al.* (2004)
$Rb(UO_2)F(HPO_4)$		$Cmc2_1$	uuuu	Ok *et al.* (2006)
$Cs_2(UO_2)_2F_2(HPO_4)_2(H_2O)$		$Pca2_1$	uuuuddd	Ok *et al.* (2006)
$Mg(H_2O)_6[(UO_2)_2(CrO_4)_2(OH)_2](H_2O)_3$		$Cmcm$	ddudd, uuduu	Unruh *et al.* (2012)
$Co(H_2O)_4(Co(H_2O)_6)_2[(UO_2)_4(CrO_4)_6(OH)_2](H_2O)_8$		$P2_1/n$	dudduuu, uduuddd	Unruh *et al.* (2012)

bonds from Mg to the sheets, which are too distant, an additional three non-transformer groups are located in the interlayer. In the highly complex interlayer of synthetic $Co(H_2O)_4(Co(H_2O)_6)_2[(UO_2)_4(CrO_4)_6(OH)_2](H_2O)_4$, there are transformer H_2O groups coordinated to two symmetrically distinct Co^{2+} cations, and an additional four non-transformer H_2O groups, which propagate bonds to the sheets. In deliensite there are five transformer H_2O groups bonded to Fe^{2+} and two additional non-transformer groups, which is one more transformer group per cation. The different hydrogen-bonding scheme is also reflected in the orientation of the bond-valence acceptors within the sheets, non-bridging vertices (oxygen atoms) of the tetrahedral units and apical uranyl oxygen atoms. This phenomenon also affects the general symmetry of the compound as discussed in the following text.

Geometrical isomerism

The structure sheets of the compounds described in the preceding section are based on the phosphuranylite anion topology (Burns, 2005). General aspects of this topology, with regard to the stereochemistry of the interlayer complex, have been discussed in detail by Schindler and Hawthorne (2008). Sheets based on phosphuranylite topology contain hexagons, pentagons, squares and triangles, and in the case of the discussed compounds, the hexagons are vacant. The ring symbol for such a topology is $6^1 5^2 4^2 3^2$ (Krivovichev and Burns, 2007). In addition to topological isomerism, which reflects differences in the bonding of the fundamental units (e.g. monodentate *vs*. bidentate linkages and edge- or corner-sharing within the chain/sheet) and which is uniquely reflected in the graphical representation of the topology, 2D structural sheets of the uranyl compounds also exhibit geometrical isomerism (Krivovichev, 2010). This phenomenon arises from the differing geometrical orientation of the TO_4 (in general) groups within the structure unit of the same composition (i.e. topology and corresponding graph). The notations of orientation or orientation matrices were introduced in order to describe such 2D units more precisely (Krivovichev, 2004, 2009, 2010; Krivovichev and Burns, 2007). The sheet units, which have a general formula $[(UO_2)_x(TO_4)_x(B)_x]^{x-}$ (where x = 1, 2; T = S, Cr; and B = F, OH), found in all the compounds described in the preceding text are

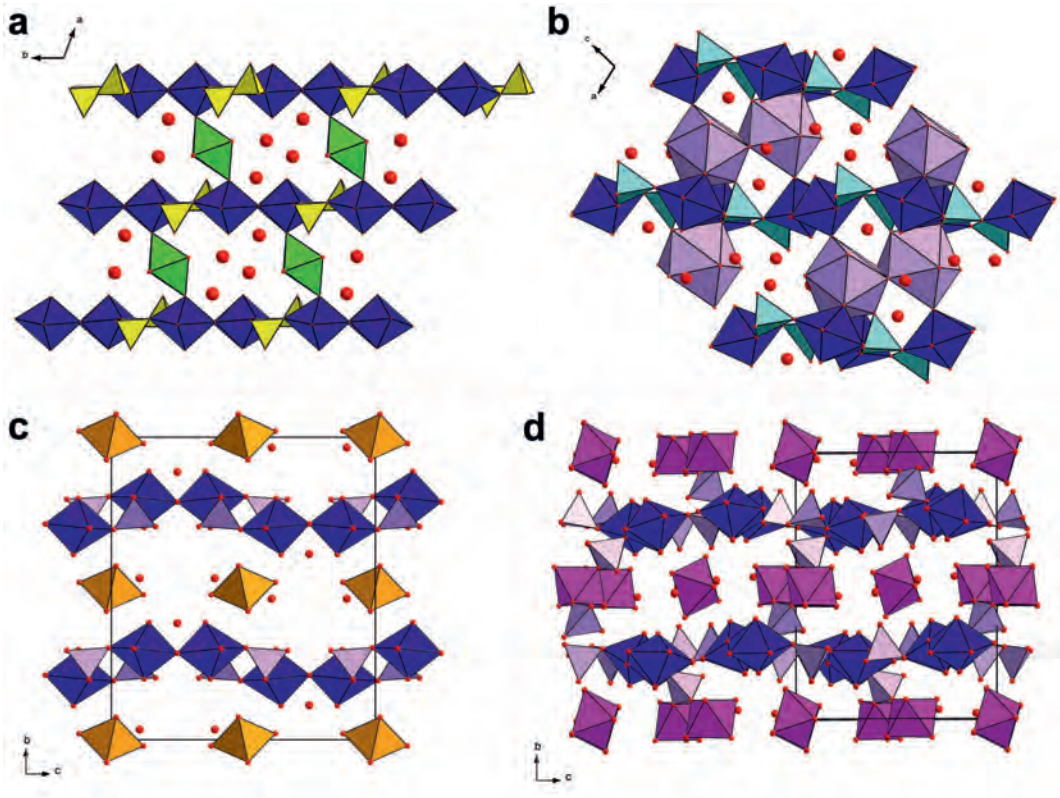

FIG. 13. (*a*) Crystal structure of johannite after Mereiter (1982); uranyl sulfate sheets are separated by an interlayer containing distorted copper octahedra (green). (*b*) Crystal structure of synthetic $Sr[(UO_2)_2(CrO_4)_2(OH)_2](H_2O)_8$ after Serezhkin *et al.* (1982); Sr-based polyhedra polymerize to form $Sr_2\Phi_{16}$ dimers. (*c*) Crystal structure of synthetic $Mg(H_2O)_6[(UO_2)_2(CrO_4)_2(OH)_2](H_2O)_3$ after Unruh *et al.* (2012); uranyl chromate layers are separated by an interlayer containing $Mg\Phi_6$ octahedra (orange) and H_2O groups which are not bonded to any cation. (*d*) Crystal structure of synthetic $Co(H_2O)_4(Co(H_2O)_6)_2[(UO_2)_4(CrO_4)_6(OH)_2](H_2O)_8$ after Unruh *et al.* (2012); uranyl chromate layers (with the third, Cr3 tetrahedron staggered towards the interlayer) are separated by a complex interlayer where two types of $Co\Phi_6$ octahedra and H_2O groups are located.

related by geometrical isomerism. The orientation notations for particular sheets are listed in Table 9. The structure sheet in deliensite is depicted in Fig. 14*a*, with a graphical representation and the orientation matrix of the SO_4 units in Fig. 14*b*. One of the simplest orientations of the TO_4 groups in sheet with the phosphuranylite topology produces the structure of johannite (Mereiter, 1982), which has a ...*udud*... sequence (Table 9; Fig. 14*c*). An identical geometrical isomer to deliensite (Table 9) was reported by Unruh *et al.* (2012) in the synthetic uranyl chromate compound $Mg(H_2O)_6[(UO_2)_2(CrO_4)_2(OH)_2](H_2O)_3$. A second compound synthesized by Unruh *et al.* (2012) is much more complex (Table 9; Fig. 14*d*). Krivovichev (2010) showed that the system of orientation of TO_4 groups in different geometrical isomers may be chiral, producing compounds that crystallize in chiral space groups (Krivovichev *et al.*, 2006, 2009); however, in this case the space group *Pnn*2 is achiral (Jones, 1986). Krivovichev (2010) further noted that the occurrence of geometrical isomers in uranyl chromate hydrates (Krivovichev and Burns, 2003) is related to the number of H_2O groups in the structure, and thus to features of the hydrogen-bonding system. The H_2O content of deliensite is different from the compounds described in the preceding paragraphs; the orientation of the TO_4 groups is closely related to the way in which are these units are involved in

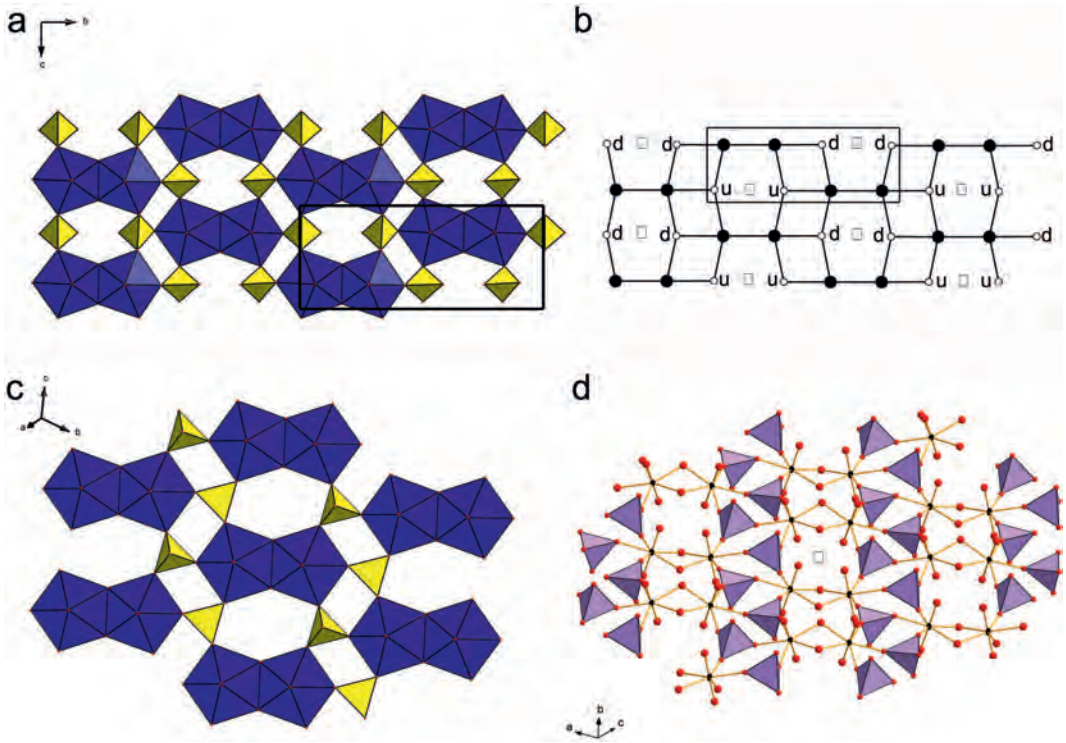

FIG. 14. (*a*) Uranyl sulfate structure sheet with the phosphuranylite topology found in deliensite and (*b*) a black (U atom) and white (S atom) graph representation of the topology using u, d and □ symbols. The orientation matrix is outlined by solid line. (*c*) Uranyl sulfate sheet in the structure of johannite (Mereiter, 1982). (*d*) Uranyl chromate sheet in the structure of synthetic $Co(H_2O)_4(Co(H_2O)_6)_2[(UO_2)_4(CrO_4)_6(OH)_2](H_2O)_8$ (Unruh *et al*., 2012); with the Cr3 tetrahedron omitted; CrO_4 are pink, U atoms black, O atoms red.

the hydrogen-bond network and to the number and strength of bonds that O atoms in the TO_4 groups accept.

Acknowledgements

We thank Jan Vylita (Prague) and Jaroslav Hyršl (Prague) who kindly provided samples for the study. We are grateful to Lukáš Palatinus and Michal Dušek (ASCR v.v.i., Prague) for discussions on the symmetry of deliensite. We also thank Pierre Vonlanthen (University of Lausanne) for his help during SEM-imaging sessions. Tom Caradoc-Davies is thanked for help in collecting synchrotron data. We are most grateful to Jana Ederová (Institute of Chemical Technology, Prague) in performing thermal analyses. Pavel Škácha (Mining Museum, Příbram) is acknowledged for providing us with marvellous photomicrographs of deliensite samples. We are grateful to Sergey Krivovichev, for his valuable review of the paper and also for the comments of anonymous reviewer. Both helped us improve the early version of the manuscript. This work was supported by the Premium Academiae and the grant of the Czech Science Foundation (P204/11/0809) to VP, KF and JP. Further support was provided by the long term Research Plan of the Ministry of Education of the Czech Republic MSM0021622412 (INCHEMBIOL) to RŠ, as well as the long-term project of the Ministry of Culture of the Czech Republic (MK00002327201) to JS and JČ.

References

Bartlett, J.R. and Cooney, R.P. (1989) On the determination of uranium-oxygen bond lengths in dioxouranium(VI) compounds by Raman spectroscopy. *Journal of Molecular Structure*, **193**,

295–300.

Birch, W.D., Mills, S.J., Maas, R. and Hellstrom, J.C. (2011) A chronology for Late Quaternary weathering in the Murray Basin, southeastern Australia: evidence from ^{230}Th/U dating of secondary uranium phosphates in the Lake Boga and Wycheproof granites, Victoria. *Australian Journal of Earth Sciences*, **58**, 835–845.

Brown, I.D. (1981) The bond-valence method: an empirical approach to chemical structure and bonding. Pp. 1–30 in: *Structure and Bonding in Crystals II* (M. O'Keeffe and A. Navrotsky, editors). Academic Press, New York.

Brown, I.D. (2002) *The Chemical Bond in Inorganic Chemistry: The Bond Valence Model*. Oxford University Press, Oxford, UK, 230 pp.

Brown, I.D. and Altermatt, D. (1985) Bond-valence parameters obtained from a systematic analysis of the inorganic crystal structure database. *Acta Crystallographica*, **B41**, 244–247, [including updated parameters from http://www.ccp14.ac.uk/ccp/web-mirrors/i_d_brown/].

Brown, I.D. and Shannon, R.D. (1973) Empirical bond-strength bond-length curves for oxides. *Acta Crystallographica*, **A29**, 266–282.

Brugger, J., Burns, P.C. and Meisser, N. (2003) Contribution to the acid drainage of uranium minerals: marecottite and the zippeite group. *American Mineralogist*, **88**, 676–685.

Burns, P.C. (2001) A new uranyl sulfate chain in the structure of uranopilite. *The Canadian Mineralogist*, **39**, 1139–1146.

Burns, P.C. (2005) U^{6+} minerals and inorganic compounds: insights into an expanded structural hierarchy of crystal structures. *The Canadian Mineralogist*, **43**, 1839–1894.

Burns, P.C., Ewing, R.C. and Hawthorne, F.C. (1997) The crystal chemistry of hexavalent uranium: polyhedron geometries, bond-valence parameters, and polymerization of polyhedra. *The Canadian Mineralogist*, **35**, 1551–1570.

Caubel, P. (1998) Le Mas Lavayre, Hérault, un deuxième gîte de deliensite. *Le Règne Minéral*, **22**, 14–17.

Čejka, J. (1999) Infrared spectroscopy and thermal analysis of the uranyl minerals. Pp. 521–622 in: *Uranium: Mineralogy, Geochemistry and the Environmen*t (P.C. Burns and R. Finch, editors). Reviews in Mineralogy, **38**. Mineralogical Society of America, Washington DC.

Čejka, J. (2004) Vibrational spectroscopy of uranyl minerals – infrared and Raman spectra of uranyl minerals. I. Uranyl, UO_2^{2+}. *Bulletin mineralogicko-petrologického Oddělení Národního Muzea (Praha)*, **12**, 44–51, [in Czech].

Čejka, J. (2007) Vibrational spectra of uranyl minerals – infrared and Raman spectra of uranyl minerals. III. Uranyl sulphates. *Bulletin mineralogicko-petrologického Oddělení Národního Muzea (Praha)*, **14–15**, 40–46, [in Czech].

Čejka, J., Urbanec, Z., Čejka, J. Jr and Mrázek, Z. (1988) Contribution to the thermal analysis and crystal chemistry of johannite $Cu[(UO_2)_2(SO_4)_2(OH)_2]\cdot 8H_2O$. *Neues Jahrbuch für Mineralogie, Abhandlungen*, **159**, 297–309.

Chapot, G., Couprie, R., Dumas, J., Leblanc, P. and Kerouanton, J.-L. (1996) L'uranium Vendéen, 40 ans de recherches et d'exploitations minières dans le Massif Armoricain. *Cahiers du Patrimoine*, **45**, 176–187.

Chen, F., Ewing, R.C. and Clark, S.B. (1999) The Gibbs free energies and enthalpies of formation of U^{6+} phases: an empirical method of prediction. *American Mineralogist*, **84**, 650–664.

Deditius, A.P., Utsunomiya, S. and Ewing, R.C. (2008) The chemical stability of coffinite, $USiO_4\cdot nH_2O$; $0<n<2$, associated with organic matter: a case study from Grants uranium region, New Mexico, USA. *Chemical Geology*, **251**, 33–49.

Doran, M.B., Cockbain, B.E. and O'Hare, D. (2005) Structural variation in organically templated uranium sulfate uorides. *Dalton Transactions*, **2005**, 1774–1780.

Finch, R.J. and Murakami, T. (1999) Systematics and paragenesis of uranium minerals. Pp. 91–179 in: *Uranium: Mineralogy, Geochemistry and the Environmen*t (P.C. Burns and R. Finch, editors). Reviews in Mineralogy, **38**. Mineralogical Society of America, Washington DC.

Frost, R.L. and Čejka, J. (2009) A Raman spectroscopic study of the uranyl mineral rutherfordine – revisited. *Journal of Raman Spectroscopy*, **40**, 1096–1103.

Halasyamani, P.S., Francis, R.J., Walker, S.M. and O'Hare, D. (1999) New layered uranium(VI) molybdates: syntheses and structures of $(NH_3(CH_2)_3NH_3)(H_3O)_2(UO_2)_3(MoO_4)_5$, $C(NH_2)_3(UO_2)(OH)(MoO_4)$, $(C_4H_{12}N_2)(UO_2)(MoO_4)_2$, and $(C_5H_{14}N_2)(UO_2)(MoO_4)_2\cdot H_2O$. *Inorganic Chemistry*, **31**, 278–279.

Holland, T. and Redfern, S.A.T. (1997) Unit cell refinement from powder diffraction data: the use of regression diagnostics. *Mineralogical Magazine*, **61**, 65–77.

Hooft, R.W.W., Straver, L.H. and Spek, A.L. (2008) Determination of absolute structure using Bayesian statistics on Bijvoet differences. *Journal of Applied Crystallography*, **41**, 96–103.

Hoppe, R. (1979) Effective coordination number (ECoN) and mean-fictive ionic radii (Mefir). *Zeitschrift für Kristallographie*, **150**, 23–52.

Jensen, K.A., Palenik, C.S. and Ewing, R.C. (2002) U^{6+} phases in the weathering zone of the Bangombé U-

deposit: observed and predicted mineralogy. *Radiochimica Acta*, **90**, 761–769.

Jones, P.G. (1986) The determination of absolute structure. III. An ambiguity table for the non-centrosymmetric crystal classes. *Acta Crystallographica*, **A42**, 57.

Krivovichev, S.V. (2004) Combinatorial topology of salts of inorganic oxoacids: zero-, one- and two dimensional units with corner-sharing between coordination polyhedra. *Crystallography Reviews*, **10**, 185–232.

Krivovichev, S.V. (2009) *Structural Crystallography of Inorganic Oxysalts*. Oxford University Press, Oxford, UK, 320 pp.

Krivovichev, S.V. (2010) Actinyl compounds with hexavalent elements (S, Cr, Se, Mo) – structural diversity, nanoscale chemistry, and cellular automata modelling. *European Journal of Inorganic Chemistry*, **2010**, 2594–2603.

Krivovichev, S.V. and Burns, P.C. (2003) Geometrical isomerism in uranyl chromates I. Crystal structures of $(UO_2)(CrO_4)(H_2O)_2$, $[(UO_2)(CrO_4)(H_2O)_2](H_2O)$ and $[(UO_2)(CrO_4)(H_2O)_2]_4(H_2O)_9$. *Zeitschrift für Kristallographie*, **218**, 568–574.

Krivovichev, S.V. and Burns, P.C. (2007) Actinide compounds containing hexavalent cations of the VI group elements (S, Se, Mo, Cr, W). Pp. 95–182 in: *Structural Chemistry of Inorganic Actinide Compounds* (S.V. Krivovichev, P.C. Burns and I.G. Tananaev, editors). Elsevier, Amsterdam.

Krivovichev, S.V., Gurzhii, V.V., Tananaev, I.G. and Myasoedov, B.F. (2006) Topology of inorganic complexes as a function of amine molecular structure in layered uranyl selenates. *Doklady Physical Chemistry*, **409**, 228–232.

Krivovichev, S.V., Gurzhii, V.V., Tananaev, I.G. and Myasoedov, B.F. (2009) Amine-templated uranyl selenates with chiral $[(UO_2)_2(SeO_4)_3(H_2O)]^{2-}$ layers: topology, isomerism, structural relationships. *Zeitschrift für Kristallographie*, **224**, 316–324.

Lane, M.D. (2007) Mid-infrared emission spectroscopy of sulfate and sulfate-bearing minerals. *American Mineralogist*, **92**, 1–18.

Libowitzky, E. (1999) Correlation of O–H stretching frequencies and O–H···O hydrogen bond lengths in minerals. *Monatshefte für Chemie*, **130**, 1047–1059.

Meisser, N., Brugger, J. and Lahaye, Y. (2002) Mineralogy and acid-mine drainage of La Creusaz uranium prospect, Switzerland. Pp. 147–150 in: *Uranium Deposits: From their Genesis to the Environmental Aspects, Proceedings* (B. Kříbek and J. Zeman, editors). Czech Geological Survey, Prague.

Mereiter, K. (1982) Die Kristallstrukturs des Johannits, $Cu(UO_2)_2(OH)_2(SO_4)_2 \cdot 8H_2O$. *Tschermaks Mineralogische und Petrologisches Mitteilungen*, **30**, 47–57.

Mereiter, K. (1986) Crystal structure and crystallographic properties of a schröckingerite from Joachimsthal. *Tschermaks Mineralogischen und Petrographischen Mitteillungen*, **35**, 1–18.

Mills, S.J., Birch, W.D., Kolitsch, U., Mumme, W.G. and Grey, I.E. (2008*a*) Lakebogaite, $CaNaFe_2^{3+}H(UO_2)_2(PO_4)_4(OH)_2(H_2O)_8$, a new uranyl phosphate with a unique crystal structure from Victoria, Australia. *American Mineralogist*, **93**, 691–697.

Mills, S.J., Birch, W.D., Maas, R., Phillips, D. and Plimer, I.R. (2008*b*) Lake Boga Granite, north-western Victoria: mineralogy, geochemistry and geochronology. *Australian Journal of Earth Sciences*, **55**, 281–299.

Nakamoto, K. (1986) *Infrared and Raman Spectra of Inorganic and Coordination Compounds*. John Wiley and Sons, New York.

Oelkers, E.H. and Montel, J. (2008) Phosphates and nuclear waste storage. *Elements*, **4**, 113–116.

Ok, K.M., Baek, J., Halasyamani, P.S. and O'Hare, D. (2006) New layered uranium phosphate fluorides: syntheses, structures, characterizations, and ion-exchange properties of $A(UO_2)F(HPO_4) \cdot xH_2O$ (A = Cs^+, Rb^+, K^+; x = 0–1). *Inorganic Chemistry*, **45**, 10207–10214.

Ondruš, P., Veselovský, F. and Hloušek, J. (1997) A review of mineral associations and paragenetic groups of secondary minerals of the Jáchymov (Joachimsthal) ore district. *Journal of the Czech Geological Society*, **42**, 109–115.

Palatinus, L. and Chapuis, G. (2007) *Superflip* – a computer program for the solu¡tion of crystal structures by charge flipping in arbitrary dimensions. *Journal of Applied Crystallography*, **40**, 451–456.

Petříček, V., Dušek, M. and Palatinus, L. (2006) *Jana2006. The crystallographic computing system*. Institute of Physics, Prague.

Plášil, J., Sejkora, J., Čejka, J., Škácha, P., Goliáš, V., Pavlíček, R. and Hofman, P. (2008) Supergene mineralization from the dump of the uranium shaft no. 16 Háje (Příbram). *Bulletin Mineralogicko-petrologického oddělení Národního Muzea (Praha)*, **16**, 43–55, [in Czech].

Plášil, J., Dušek, M., Novák, M., Čejka, J., Císařová, I. and Škoda, R. (2011*a*) Sejkoraite-(Y), a new member of the zippeite group containing trivalent cations from Jáchymov (St. Joachimsthal), Czech Republic: description and crystal structure refinement. *American Mineralogist*, **96**, 983–991.

Plášil, J., Mills, S.J., Fejfarová, K., Dušek, M., Novák, M., Škoda, R., Čejka, J. and Sejkora, J. (2011*b*) The crystal structure of natural zippeite, $K_{1.85}H^+_{0.15}[(UO_2)_4O_2(SO_4)_2(OH)_2](H_2O)_4$, from Jáchymov, Czech Republic. *The Canadian*

Mineralogist, **49**, 1089–1103.

Plášil, J., Hloušek, J., Veselovský, F., Fejfarová, K., Dušek, M., Škoda, R., Novák, M., Čejka, J., Sejkora, J. and Ondruš, P. (2012*a*) Adolfpateraite, $K(UO_2)(SO_4)(OH)(H_2O)$, a new uranyl sulfate mineral from Jáchymov, Czech Republic. *American Mineralogist*, **97**, 447–454.

Plášil, J., Fejfarová, K., Wallwork, K.S., Dušek, M., Škoda, R., Sejkora, J., Čejka, J., Veselovský, F., Hloušek, J., Meisser, N. and Brugger, J. (2012*b*) Crystal structure of pseudojohannite, with a revised formula, $Cu_3(OH)_2[(UO_2)_4O_4(SO_4)_2](H_2O)_{12}$. *American Mineralogist*, **97**, 1796–1803.

Plášil, J., Fejfarová, K., Škoda, R., Dušek, M., Marty, J. and Čejka, J. (2012*c*) The crystal structure of magnesiozippeite, $Mg[(UO_2)_2O_2(SO_4)](H_2O)_{3.5}$, from East Saddle Mine, San Juan County, Utah (U.S.A.). *Mineralogy and Petrology*, http://dx.doi.org/10.1007/s00710-012-0241-7.

Pouchou, J.L. and Pichoir, F. (1985) "PAP" (φρZ) procedure for improved quantitative microanalysis. Pp. 104–106 in: *Microbeam Analysis* (J.T. Armstrong, editor). San Francisco Press, San Francisco, California, USA.

Robinson, K., Gibbs, G.V. and Ribbe, P.H. (1971) Quadratic elongation: a quantitative measure of distortion in coordination polyhedra. *Science*, **172**, 567–570.

Schindler, M. and Hawthorne, F.C. (2008) The stereochemistry and chemical composition of interstitial complexes in uranyl-oxysalt minerals. *The Canadian Mineralogist*, **46**, 467–501.

Serezhkin, V.N., Boiko, N.V. and Trunov, V.K. (1982) Crystal structure of $Sr[UO_2(OH)CrO_4]_2 \cdot 8H_2O$. *Journal of Structure Chemistry*, **23**, 270–273.

Sokol, F. and Čejka, J. (1992) A thermal and mass spectrometric study of synthetic johannite $[Cu(UO_2)_2(SO_4)_2(OH)_2] \cdot 8H_2O$. *Thermochimica Acta*, **206**, 235–242.

Spek, A.L. (1988) *LePage* – an MS DOS program for the determination of the metrical symmetry of a translation lattice. *Journal of Applied Crystallography*, **21**, 578–579.

Spek, A.L. (2003) Single-crystal structure validation with the program *PLATON*. *Journal of Applied Crystallography*, **36**, 7–13.

Spek, A.L. (2009) Structure validation in chemical crystallography. *Acta Crystallographica*, **D65**, 148–155.

Tali, R., Tabachenko, V.V., Kovba, L.M. and Dem'yanets, L.N. (1994) Structure of some uranyl hydroxomolybdates. *Zhurnal Neorganicheskoi Khimii*, **39**, 1752–1754, [in Russian].

Unruh, D.K., Baranay, M., Pressprich, L., Stoffer, M. and Burns, P.C. (2012) Synthesis and characterization of uranyl chromate sheet compounds containing edge-sharing dimers of uranyl pentagonal bipyramids. *Journal of Solid State Chemistry*, **186**, 158–164.

Vochten, R., Blaton, N. and Peeters, O. (1997) Deliensite, $Fe(UO_2)_2(SO_4)_2(OH)_2 \cdot 3H_2O$, a new ferrous uranyl sulfate hydroxy hydrate from Mas d'Alary, Lodève, Hérault, France. *The Canadian Mineralogist*, **35**, 1021–1025.